INTERPOLATION AND RANGE EXTRAPOLATION OF SOUND SOURCE DIRECTIVITY BASED ON A SPHERICAL WAVE PROPAGATION MODEL

Jens Ahrens

Audio Technology Group
Division of Applied Acoustics
Chalmers University of Technology
412 96 Gothenburg, Sweden
jens.ahrens@chalmers.se

Stefan Bilbao

Acoustics and Audio Group
Reid School of Music
University of Edinburgh
Edinburgh, United Kingdom
s.bilbao@ed.ac.uk

ABSTRACT

Approaches for incorporating sound source directivity into wave-based room acoustic simulations using a spherical harmonic representation have been presented recently. Normally, the directivity is measured or prescribed on a spherical surface centered at the nominal source position. In wave-based simulations, this directivity can be represented through a locally-defined driving term acting at the source location. In practice, the directivity of real-world sound sources like musical instruments or industrial machinery can only be measured approximately in terms of spatial resolution and accuracy. We show that the measurement data can be augmented such that the impairments due to the limitations of the measurement accuracy are mitigated. We revisit the previously proposed approach of only using the angle-dependent magnitude of the measured directivity together with a spherical-wave propagation model and demonstrate its potential by means of numerical simulations based on two case studies.

Index Terms— Radiation, directivity, spherical harmonics, wave-based room simulation

1. INTRODUCTION

The measurement and modelling of sound source directivity has seen increased interest in recent years. The main application areas are the analysis of the directivity of, for example, musical instruments in order to understand the impact on the listening experience [1], how the directivity interacts with room acoustics [2], and how noise from machinery propagates in a given environment [3], or virtual reality [4]. Simple models for directivity include [5].

Spherical harmonics (SH) have been shown to be a powerful representation of sound source directivity [6, 7], going back to early work by Weinreich [8]. We will focus on wave-based room acoustical simulations such as [9] as an application scenario in the present paper because it is this case that places the most stringent requirements on the modelling of the sound source directivity as the entire range of the directivity from the nominal source position to very far distances needs to be modelled.

The incorporation of source directivity into geometrical acoustics has seen some investigation. Spatial resolution of source directivity was studied in [2]; a significant impact of the maximum SH order of the directivity on room acoustical metrics was found with saturation occurring at an SH order of around 10. It was found in [10] that directivities of order higher than 4 were not perceptually significant in a binaural auralization of an image-source-based room simulation.

A major challenge is the measurement of directivities of sources that are not electroacoustical transducers. This is mainly because it is not possible with most sources to drive them in a reproducible manner with a known input signal as in the case of, e.g., musical instruments or machinery. Musical instrument directivities presented in [11] were measured using a spherical array of 32 microphones surrounding a musician playing a scale at different dynamic levels. Stable partial oscillations were identified and the magnitude and phase at each microphone position was deduced manually. Alternative methods for determining the data were presented for the same data set in [12]. Either way, such measurements are too sparse with respect to frequency to, for example, perform an inverse Fourier transform to obtain an impulse response representation. The phase of such a directivity can change strongly with the playing style and dynamics [6] so it should also be assumed that the phase data are unreliable. Similar if not stronger limitations apply to the measurement of the directivity of machinery and the like.

Conceptually, the directivity represents a whole set of information, including the location of a radiating surface, the time-frequency information as well as the propagation of the radiated sound field. The limitations of the measurement procedures do not allow all this information to be deduced from the data. Here, we will extract only the magnitude information with respect to both angle and frequency from the measurement data and impose all remaining information manually. We propose to impose source position and curvature of the wave front by means of a spherical wave model. This source model was already employed in the modeling of the directivity of moving sources in [13] and with the boundary element method in [4], but its properties were not investigated further. We demonstrate the usefulness of this choice in the present paper.

Source directivity and a far-field approximation are outlined in Sec. 2. FDTD methods are briefly introduced in Sec. 3. Numerical results, illustrating the incorporation of source directivity data into an FDTD simulation are shown in Sec. 4.

2. SOURCE DIRECTIVITY AND AN APPROXIMATION

The term *directivity* with regard to acoustic sources has been defined in various ways in the literature [14, 15, 16], [17, p. 204]. Here, we define directivity as the spatio-temporal transfer function (STTF) of a sound source under free-field conditions, evaluated at arbitrary spatial locations. This is the most general definition, from which the others above can be derived. We will assume that the directivity is evaluated on a spherical surface centered around the source.

A source directivity $W(r, \boldsymbol{\gamma}, \omega)$ is dependent on an angular frequency ω, in rad./sec, a radial distance r in m from the nominal source center, and an angle 3-vector $\boldsymbol{\gamma}$ defined interns of azimuth angle α and colatitude β. It is defined as

$$W(r, \boldsymbol{\gamma}, \omega) = \sum_{l=0}^{\infty} \sum_{m=-l}^{l} \underbrace{\breve{W}_{l,m}(\omega) h_l^{(1)}\left(\frac{\omega r}{c}\right)}_{=\mathring{W}_{l,m}(r,\omega)} Y_{l,m}(\boldsymbol{\gamma}) \,, \quad (1)$$

and represents the radiated acoustic field exterior to a sphere that is just large enough to completely enclose the sound source [17, p. 206]. $h_l^{(1)}(\cdot)$ is the lth order spherical Hankel function of first kind, and $Y_{l,m}(\boldsymbol{\gamma})$, defined for integer $l \geq 0$ and $-l \leq m \leq l$, are the SH basis functions, which we are assuming to be purely real. $\breve{W}_{l,m}(\omega)$ are coefficients that contain all information about the source directivity.

The coefficients $\breve{W}_{l,m}(\omega)$ follow from an approximation to

$$\breve{W}_{l,m}(\omega) = \frac{1}{h_l^{(1)}\left(\frac{\omega R}{c}\right)} \iint_{S^2} W(R, \boldsymbol{\gamma}, \omega) Y_{l,m}(\boldsymbol{\gamma}) d\Omega \,, \quad (2)$$

where $W(R, \gamma, \omega)$ is a directivity known on a spherical surface with radius R that encloses the source, and S^2 represents the unit sphere. Alternatively, a least-squares fit of the coefficients to the spatially discrete measurement data points can be performed based on (1) [18, 19, 9]. In either case, only the coefficients up to a given order $l = L$ that depends on the number of measurement points can be obtained.

Evaluating the directivity in the limit of $r \to \infty$ [17, p. 204], leads to the large-argument approximation of the spherical Hankel function given by (12), and (1) simplifies to [17, p. 204]

$$W_\infty(r, \boldsymbol{\gamma}, \omega) = \frac{\mathrm{e}^{\mathrm{i}\frac{\omega r}{c}}}{r} \frac{c}{\mathrm{i}\omega} \sum_{l=0}^{\infty} \sum_{m=-l}^{l} (-\mathrm{i})^l \breve{W}_{l,m}(\omega) Y_{l,m}(\boldsymbol{\gamma}) \,. \quad (3)$$

$W_\infty(r, \boldsymbol{\gamma}, \omega)$ is referred to as the *far-field signature* of the directivity [20, p. 81]. Eq. (3) tells us that at sufficient distance, a source of finite spatial extent radiates spherical wave fronts ($e^{\mathrm{i}\frac{\omega r}{c}}/r$), the complex amplitude of which depends on the angle and is represented by the coefficients $\breve{W}_{l,m}(\omega)$. In other words, the angular dependence of the directivity is imposed onto a spherical wave. How far this sufficient distance has to be depends on the spatial extent of the source and its distance from the coordinate origin (which coincides with the nominal location of the source). The observation distance has to be much larger than the largest dimension of the source. Classical polar diagrams display the magnitude of the far-field signature $W_\infty(r, \boldsymbol{\gamma}, \omega)$.

The origin of the wave fronts in (3) is sometimes called the *acoustical center* of the source [21]. It was highlighted in [6, 22, 23] that in directivity measurements, the source should be located in the center of the enclosing spherical array in order to concentrate energy in the lower SH orders. Source centering has been proposed ibidem, which consists in identifying the acoustic centers of the elementary sound sources that the source comprises (one is assumed for each frequency bin) and placing the coordinate origin into the acoustic centers. This procedure tends to be successful only at lower frequencies ($<$ 1 kHz) where no spatial aliasing is apparent [11].

Because of the limitations of directivity measurement data highlighted in Sec. 1, we follow the proposition from [13] to impose the nominal source location as well as a model of the propagation (particularly the radial dependency) on the measured data using (3), an approach which is justifiable at large distances. If the source is of small spatial extent and located at the origin of the coordinate system, the discrepancy will be very small. This assumption holds for most sound sources for which detailed directivity data is available, such as [11] (which also includes virtual source centering as mentioned above). We will demonstrate the usefulness of this choice via numerical simulations in Sec. 4.

As the phase data cannot be measured reliably and are often too sparse to perform interpolation, we here extract only the magnitude of the directivity from the measurement data and impose it onto a spherical wave that originates from the coordinate origin [4]. We use the symbol $W'(r, \boldsymbol{\gamma}, \omega)$ in the remainder of this paper to represent this new modeled directivity. More precisely, $W'(R, \boldsymbol{\gamma}, \omega)$ over the spherical measurement surface of radius R is given by

$$W'(R, \boldsymbol{\gamma}, \omega) = \frac{\mathrm{e}^{\mathrm{i}\frac{\omega R}{c}}}{R} R \cdot |W(R, \boldsymbol{\gamma}, \omega)| \,, \quad (4)$$

whereby multiplication by the radius R is employed for normalisation. Expressing the angular part in (4) based on SH leads to

$$W'(R, \boldsymbol{\gamma}, \omega) = \mathrm{e}^{\mathrm{i}\frac{\omega R}{c}} \sum_{l=0}^{\infty} \sum_{m=-l}^{l} \breve{W}'_{l,m}(\omega) Y_{l,m}(\boldsymbol{\gamma}) \,. \quad (5)$$

To obtain the SH coefficients $\mathring{W}'_{l,m}(R, \omega)$ of the complete model of $W'(r, \boldsymbol{\gamma}, \omega)$ as per (1), we constrain the magnitude of $W'(r, \boldsymbol{\gamma}, \omega)$ to be equal to the magnitude of the measured directivity $W(r, \boldsymbol{\gamma}, \omega)$ on the measurement surface as

$$|W(R, \boldsymbol{\gamma}, \omega)| = \sum_{l=0}^{\infty} \sum_{m=-l}^{l} \breve{W}'_{l,m}(\omega) Y_{l,m}(\boldsymbol{\gamma}) \,. \quad (6)$$

Eq. (6) may be solved for $\breve{W}'_{l,m}(\omega)$ either using (2) (without dividing by $h_l^{(1)}(\cdot)$) or performing a least-squares fit [4]. As before, this can be achieved only up to a certain order $l = L$ in practice.

The coefficients $\mathring{W}'_{l,m}(R, \omega)$ of the complete SH based model of $W'(r, \boldsymbol{\gamma}, \omega)$ are given by

$$\mathring{W}'_{l,m}(R, \omega) = \mathrm{e}^{\mathrm{i}\frac{\omega R}{c}} \breve{W}'_{l,m}(\omega) \,, \quad (7)$$

and, finally, using [17, Eq. (6.94)]

$$W'(r, \boldsymbol{\gamma}, \omega) = \sum_{l=0}^{\infty} \sum_{m=-l}^{l} \mathring{W}'_{l,m}(R, \omega) \frac{h_l^{(1)}\left(\frac{\omega r}{c}\right)}{h_l^{(1)}\left(\frac{\omega R}{c}\right)} Y_{l,m}(\boldsymbol{\gamma}) \,. \quad (8)$$

It may be advantageous to fit a given desired phase to the magnitude directivity $|W(R, \gamma, \omega)|$ obtained via (6) such as minimum phase or linear phase [24] to design the time-domain structure of the signals. Also, augmentation of the data through recovery of the algebraic sign of lobes in the directivity as proposed in [25] may be applied.

3. INTEGRATION INTO WAVE SIMULATIONS

Volumetric wave-based acoustic simulation dates back to the 1990s [26, 27, 28], and can be viewed as a more accurate alternative to geometric acoustics simulation, in that all effects of diffraction are modelled. Though computationally intensive, simulations for reasonable-sized spaces at audio rates are possible nowadays [29]. The finite difference time domain method (FDTD) is one particular type of wave-based method that will be employed here.

In contrast with most other applications, the incorporation of source directivity into wave-based room acoustical simulations like FDTD as proposed, for example, in [9] requires extrapolation of the directivity to a nominal position for a driving term, which coincides with the origin of the coordinate system in (1). Strictly speaking, (1) is a so-called exterior representation that is only valid outside of a sphere that contains the sound source in its entire extent [17, p. 206]. By extrapolating the directivity to the center of the coordinate system, we actually penetrate the sound source whose directivity we are considering. The consequence is that the directivity will not be meaningful when evaluated at such interior positions. However, (1) is a physically viable solution to the wave equation even in the interior domain so that we are not facing fundamental physical limitations here.

The numerical conditioning of the involved quantities deserves attention particularly in view of the fact that source directivities have a singularity at the source position (the directivity of a point source (a 0th-order directivity) is $\propto 1/r$, and that of a dipole (a 1st-order directivity) is $\propto \omega^2/r^2$ [17, p. 198, 200]; cf. also [30, p. 40]). Also, the far-field signature (3) comprises multiple time integrations (represented by the factor $1/\mathrm{i}\omega$), which diverge at low frequencies.

We here investigate the numerical conditioning of the signals through which the sound source directivity is injected into the simulation framework. It is shown in [9] that a directivity that is available as a set of SH coefficients $\mathring{W}_{l,m}(R,\omega)$ (cf. (1)) over a sphere of finite radius R centered around the source can be directly substituted into an FDTD simulation, with appropriately defined SH driving terms. The input signals $\hat{a}_{l,m}(\omega)$ to the FDTD simulation can be computed via [9]

$$\hat{a}_{l,m}(\omega) = \frac{4\pi c\,(-1)^l\,\mathrm{i}^l}{(\mathrm{i}\omega)^{l+1} h_l^{(1)}\left(\frac{\omega R}{c}\right)}\,\mathring{W}_{l,m}(R,\omega)\,. \tag{9}$$

Each such signal $\hat{a}_{l,m}(\omega)$ selects the contribution of a single SH component, of indices l, m to the directivity. The signals $\hat{a}_{l,m}(\omega)$ from (9) do indeed exhibit a frequency dependence, the implications of which are not immediately obvious from the mathematical expression above. We refer the reader to Appendix A where we demonstrate that the computation of the signals $\hat{a}_{l,m}(\omega)$ is numerically well-behaved in the low frequency limit.

4. RESULTS

4.1. Case Study 1: The Displaced Monopole

It is very likely, when measuring the directivity of real-world sources, that some parts of the radiating structure cannot be placed at the center of the spherical microphone array. We illustrate in this section the consequences of this circumstance and how our presented method can mitigate against this difficulty. Note that the virtual source centering that has been proposed in [6, 22, 23] cannot be considered an ultimate cure to this due to the fact that such methods are only effective if there is only one source location per frequency bin, which will typically not be the case.

We assume in the following the simplest possible source: a monopole source that is located at $\vec{x}_s = (0.3, 0, 0)$ m whose directivity is known at 1800 equi-angularly spaced positions on a spherical surface that is centered around the coordinate origin and has a radius of $R = 1$ m. We use these simulated measurement data to extract a conventional SH representation (1) of the directivity of order $L = 6$ by means of a least-squares fit.

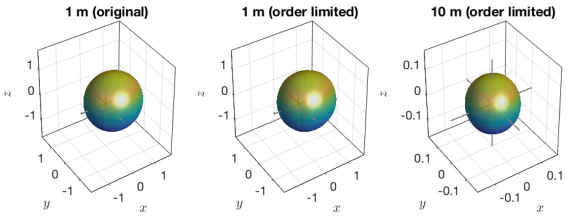

(a) Classical SH representation, Eq. (1), $f = 600$ Hz

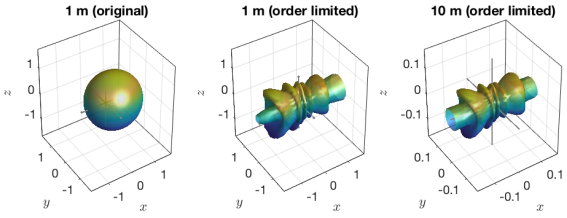

(b) Classical SH representation, Eq. (1), $f = 1500$ Hz

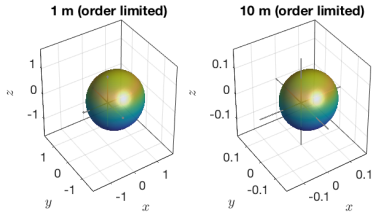

(c) Proposed representation, Eq. (5), $f = 1500$ Hz

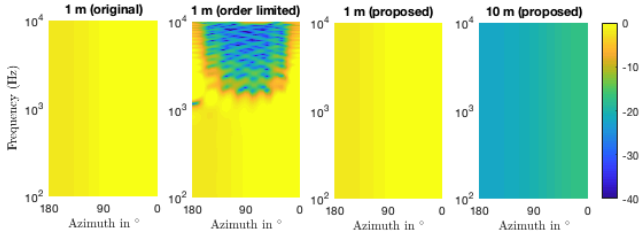

(d) From left to right: original measured; original order limited; proposed at measurement surface; proposed extrapolated

Fig. 1. Magnitude of the directivity of a 6th-order monopole displaced by 0.3 m from the coordinate origin evaluated at 1 m distance in the horizontal plane and extrapolated to 10 m distance

Fig. 1(a) and (b) illustrate the magnitude of this 6th-order directivity at two different frequencies. It can be seen that the original directivity is represented well at frequencies at which the wavelength is longer than the displacement (Fig. 1(a)). At higher frequencies as in Fig. 1(b), the order-limited representation departs substantially from the original directivity. This observation is one facet of a high-frequency roll-off that is inherent to order-limited translated SH expansions [31, 32]. The roll-off is clearly visible in Fig. 1(d). The departure is maintained when extrapolating the directivity to large distances (see the right-most plot in Fig. 1(b)). Extrapolation was performed based on (8). Note that the results are identical when using the analytical expressions of the SH representation of the displaced monopole (that are obtained via (2)) due to the orthogonality of the SH and the linear independence of the spherical Hankel functions in (1).

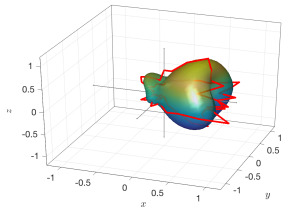

(a) Modelled directivity based on (5); the red lines connect the original measured data points

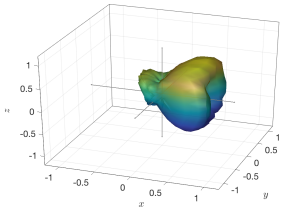

(b) Directivity at 1 m measured inside the FDTD simulation

Fig. 2. Directivity of a singing voice at $f = 2000$ Hz modeled based on a sparse set of measurement points

Our solution shown in Fig. 1(c) is capable of replicating the original magnitude directivity much better at any frequency. This circumstance is also reflected by the time-frequency magnitude spectrum of the directivity evaluated along the equator of the reference sphere as well as at a 10 m distance that is depicted in Fig. 1(d).

4.2. Case Study 2: Sparsely-measured Directivity of a Singing Voice

This example demonstrates the convenience of the proposed methods for the interpolation of directivities.

The database [33] that accompanies [34] contains recordings of two classical singers performing a glissando over one octave (i.e., a complex tone sweep). The set of partials may be interpreted as a staggered sweep over a wide frequency range so that the corresponding impulse responses can be computed via deconvolution. The recordings were made with two circular microphone arrays with 32 elements each and placed along the horizontal and median planes, respectively, at a distance of 1 m from the singer's head. Effectively, only 62 measurement points are available due to coincidence of two of the microphones. This is a very sparse set of data points for which established directivity models are not suitable. It is not possible to obtain a general directivity model as in (1) from these data. Other comparably sparse representations of sound source directivity are the Common Loudspeaker Format [15] that provides only magnitude data in 3rd-octave bands or databases for musical instrument directivities that also provide data primarily in 3rd-octave bands, [11].

We applied a combination of rotation and interpolation to the data in the file `IR_a_long_sweep.mat` to produce magnitude data points at locations all around a spherical surface. Note that such interpolation is not possible for the phase of the directivity due to the ambiguitites due to the periodicity of the phase. We then performed a least-squares fit of a 6th-order SH model according to (6) together with a minimum-phase response. The resulting directivity is shown in Fig. 2(a).

This directivity was injected via the signals $\hat{a}_{l,m}(\omega)$ given by (9) into an FDTD simulation (a simple seven-point scheme, as described in [9], and operating at 44.1 kHz). Technically, the FDTD simulation performs an extrapolation of the directivity that is a numerical approximation to (8). We still incorporate FDTD here for completeness as an application example. The directivity produced in the FDTD simulation is depicted in Fig. 2(b), and is obtained through an array of virtual microphones placed in the simulated acoustic field. The data are numerically well-conditioned, and it can be seen that the directivities coincide. This coincidence is, as expected, independent of the distance at which the directivity is evaluated inside the FDTD simulation and precise circumstances are to be investigated in future work.

5. CONCLUSIONS

We have revisited here a model for sound source directivity that is based on designing a far-field directivity such that its magnitude matches the magnitude of a near-field directivity on a spherical surface around the sound source. We have demonstrated with two case studies that this model allows two fundamental limitations of nearfield models to be overcome: 1) the high-frequency roll-off of order-limited spherical harmonics models of the directivity, and 2) the inability of establishing a model based on a sparse set of measurement points. We have also presented a first result on integrating the directivity model into time-domain wave-based room acoustic simulations.

Although a rigourous proof is not given here, there are strong indications that the proposed model leads to only minor deviations from the original directivity if the sound source is small. We will establish limits on the validity of the presented model regarding general (spatially extended) sound sources in future work.

Appendices

A. CONVERGENCE OF THE SIGNALS $\hat{a}_{l,m}(\omega)$

We study the convergence of (9) with respect to frequency in the following. Applying the large-argument approximation of the spherical Hankel function given by (12) to (9) yields

$$\hat{a}_{l,m}(\omega) = \frac{4\pi R}{(\mathrm{i}\omega)^l c} \mathrm{e}^{-\mathrm{i}\frac{\omega R}{c}} \mathring{W}_{l,m}(R,\omega), \quad \text{as} \quad \omega \to \infty\,, \tag{10}$$

which converges for high frequencies (assuming that the coefficients $\mathring{W}_{l,m}(R,\omega)$ converge).

Applying the small-argument approximation of the spherical Hankel function given by (14) to (9) yields

$$\hat{a}_{l,m}(\omega) = \frac{4\pi c\,(-1)^l\,\mathrm{i}\omega}{\mathrm{i}(2l-1)!!} \left(\frac{R}{c}\right)^2 \mathring{W}_{l,m}(R,\omega), \quad \text{as} \quad \omega \to 0\,, \tag{11}$$

which converges for low frequencies.

B. APPROXIMATIONS OF SPHERCIAL BESSEL AND HANKEL FUNCTIONS

The large argument approximation of the spherical Hankel function is given by [17, p. 197]

$$h_l^{(1)}(x) \approx (-\mathrm{i})^{l+1} \frac{\mathrm{e}^{\mathrm{i}x}}{x} \quad \text{as} \quad x \to \infty\,. \tag{12}$$

The small argument approximations of the spherical Bessel and Hankel functions are given by [17, p. 196, 197]

$$j_l(x) \approx \frac{x^l}{(2l+1)!!}\left(1 - \frac{x^2}{2(2l+3)} + \ldots\right) \quad \text{as} \quad x \to 0\,, \tag{13}$$

and

$$h_l^{(1)}(x) \approx -\mathrm{i}\frac{(2l-1)!!}{x^{l+2}} \quad \text{as} \quad x \to 0\,, \tag{14}$$

respectively.

C. REFERENCES

[1] J. Meyer, *Acoustics and the Performance of Music*, Springer, New York, 2009.

[2] J. Klein and M. Vorländer, "Simulative investigation of required spatial source resolution in directional room impulse response measurements," in *Proc. of EAA Spatial Audio Sig. Proc. Symp*, 2019, pp. 37–42.

[3] R. Janczur, E. Walerian, M. Meissner, and M. Czechowicz, "Influence of vehicle noise emission directivity on sound level distribution in a canyon street. Part II: experimental verification," *Applied Acoustics*, vol. 67, no. 7, pp. 659–679, 2006.

[4] R. Mehra, L. Antani, S. Kim, and D. Manocha, "Source and listener directivity for interactive wave-based sound propagation," *IEEE Trans. Visualization Comp. Graphics*, vol. 20, no. 4, pp. 83–94, 2014.

[5] G. Götz and V. Pulkki, "Simplified source directivity rendering in acoustic virtual reality using the directivity sample combination," in *147th Convention of the AES*, New York, NY, USA, Oct. 2019, p. 10286.

[6] F. Zotter, *Analysis and Synthesis of Sound-Radiation with Spherical Arrays*, Ph.D. thesis, University of Music and Performing Arts, Austria, 2009.

[7] M. Pollow, "Directivity patterns for room acoustical measurements and simulations," PhD thesis, RWTH Aachen, 2014.

[8] G. Weinreich and E. B. Arnold, "Method for measuring acoustic radiation fields," *J. Acoust. Soc. Am.*, vol. 68, no. 2, pp. 404–411, 1980.

[9] S. Bilbao, J. Ahrens, and B. Hamilton, "Incorporating source directivity in wave-based virtual acoustics: Time-domain models and fitting to measured data," *J. Acoust. Soc. Am.*, , no. (in press), 2019.

[10] M. Frank and M. Brandner, "Perceptual evaluation of spatial resolution in directivity patterns," in *Proc. of DAGA*, Rostock, Germany, 2019, pp. 1–4.

[11] N. Shabtai, G. Behler, M. Vorländer, and S. Weinzierl, "Generation and analysis of an acoustic radiation pattern database for forty-one musical instruments," *J. Acoust. Soc. Am.*, vol. 141, no. 2, pp. 1246–1256, 2017, Data available online at `http://dx.doi.org/10.14279/depositonce-5861.2` (Last viewed 23/09/2019).

[12] C. Anemüller and J. Herre, "Calculation of directivity patterns from spherical microphone array recordings," in *147th Convention of the AES*, New York, NY, USA, Oct. 2019, p. 10285.

[13] Jens Ahrens and Sascha Spors, "Wave field synthesis of moving virtual sound sources with complex radiation properties," *J. Acoust. Soc. Am.*, vol. 130, no. 5, pp. 2807–2816, 2011.

[14] J. Meyer, *Acoustics and the Performance of Music*, Springer, New York, 2009.

[15] CLF Group, "Common loudspeaker format," Available online at `http://www.clfgroup.org/` (Last viewed 06/05/2019), 2019.

[16] D. Blackstock, *Fundamentals of Physical Acoustics*, Wiley-Interscience, New York, NY, 2000.

[17] E. Williams, *Fourier Acoustics: Sound Radiation and Nearfield Acoustical Holography*, Academic Press, New York, 1999.

[18] D. N. Zotkin, R. Duraiswami, and N. Gumerov, "Regularized HRTF fitting using spherical harmonics," in *IEEE WASPAA*, New Paltz, NY, USA, Oct. 2009, pp. 257–260.

[19] J. Ahrens, M.k R. P. Thomas, and I. Tashev, "HRTF magnitude modeling using a non-regularized least-squares fit of spherical harmonics coefficients on incomplete data," in *Proc. of APSIPA*, Hollywood, CA, USA, December 2012, pp. 1–5.

[20] N. Gumerov and R. Duraiswami, *Fast Multipole Methods for the Helmholtz Equation in Three Dimensions*, Elsevier, Amsterdam, 2005.

[21] Finn Jacobsen, Salvador Barrera Figueroa, and Knud Rasmussen, "A note on the concept of acoustic center," *J. Acoust. Soc. Am.*, vol. 115, no. 4, pp. 1468–1473, 2004.

[22] D. Deboy and F. Zotter, "Acoustic center and orientation analysis of sound-radiation recorded with a surrounding spherical microphone array," in *Proc. of the 2nd Int. Symposium on Ambisonics and Spherical Acoustics*, Paris, France, 2010.

[23] I. Ben Hagai, M. Pollow, M. Vorländer, and B. Rafaely, "Acoustic centering of sources measured by surrounding spherical microphone arrays," *J. Acoust. Soc. Am.*, vol. 130, no. 4, pp. 2003–2015, 2011.

[24] B. Girod, R. Rabenstein, and A. Stenger, *Signals and Systems*, J.Wiley & Sons, New York, 2001.

[25] F. Zagala and F. Zotter, "Idea for sign-change retrieval in magnitude directivity patterns," in *Proc. of DAGA*, Rostock, Germany, 2019, pp. 1–4.

[26] O. Chiba, T. Kashiwa, H. Shimoda, S. Kagami, and I. Fukai, "Analysis of sound fields in three dimensional space by the time-dependent finite-difference method based on the leap frog algorithm," *J. Acoust. Soc. Japan*, vol. 49, pp. 551–562, 1993.

[27] D. Botteldooren, "Acoustical finite-difference time-domain simulation in a quasi-cartesian grid," *J. Acoust. Soc. Am.*, vol. 95, no. 5, pp. 2313–2319, 1994.

[28] D. Botteldooren, "Finite-difference time-domain simulation of low-frequency room acoustic problems," *J. Acoust. Soc. Am.*, vol. 98, no. 6, pp. 3302–3308, 1995.

[29] B. Hamilton, C. J. Webb, N. D. Fletcher, and S. Bilbao, "Finite difference room acoustics simulation with general impedance boundaries and viscothermal losses in air: Parallel implementation on multiple GPUs," in *Proc. Int. Symp. Musical Room Acoust.*, Buenos Aires, Argentina, sep 2016.

[30] J. Ahrens, *Analytic Methods of Sound Field Synthesis*, Springer, Heidelberg, Germany, 2012.

[31] R. Baumgartner, "Time domain fast-multipole translation for ambisonics," Diplom Thesis, University for Music and Dramatic Arts, Graz, 2011.

[32] N. Hahn and S. Spors, "Physical properties of modal beamforming in the context of data-based sound reproduction," in *139th Convention of the AES*, New York, NY, USA, Oct. 2015, p. 9468.

[33] M. Brandner, "DirPat Repository Element: Directivity Measurements of a Classical Singer," Available online at `https://phaidra.kug.ac.at/detail_object/o:76751` (Last viewed 09/23/2019), 2018.

[34] M. Brandner, M. Frank, and D. Rudrich, "DirPatDatabase and Viewer of 2D/3D Directivity Patterns of Sound Sources and Receivers," in *144th Convention of the AES*, Milan, Italy, May 2018, p. eBrief:425.